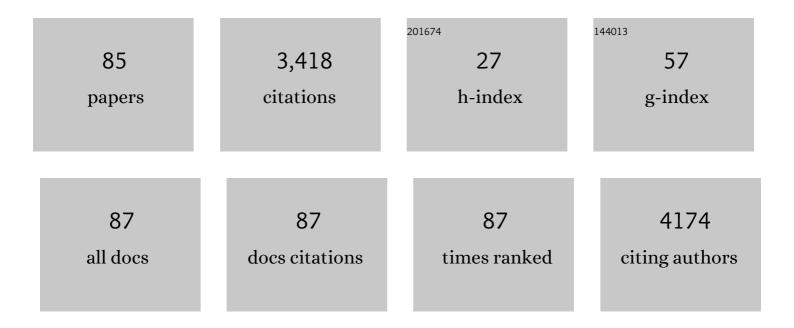
List of Publications by Year in descending order

Source: https://exaly.com/author-pdf/454661/publications.pdf Version: 2024-02-01



FUNHALEE

#	Article	IF	CITATIONS
1	Ferroelastic–Ferroelectric Multiferroicity in van der Waals Rhenium Dichalcogenides. Advanced Materials, 2022, 34, e2108777.	21.0	10
2	Hybrid Deep Learning Crystallographic Mapping of Polymorphic Phases in Polycrystalline Hf <sub>0.5</sub> Zr <sub>0.5</sub> O <sub>2</sub> Thin Films. Small, 2022, 18, e2107620.	10.0	4
3	Interaction- and defect-free van der Waals contacts between metals and two-dimensional semiconductors. Nature Electronics, 2022, 5, 241-247.	26.0	84
4	Sublayer thickness dependence of nanolaminated HfO2–Al2O3 films for ferroelectric phase stabilization. Applied Physics Letters, 2022, 120, .	3.3	4
5	Low-Dose Sparse-View HAADF-STEM-EDX Tomography of Nanocrystals Using Unsupervised Deep Learning. ACS Nano, 2022, 16, 10314-10326.	14.6	5
6	Atomic-scale identification of invisible cation vacancies at an oxide homointerface. Materials Today Physics, 2021, 16, 100302.	6.0	7
7	Sulfidation characteristics of amorphous nonstoichiometric Mo-oxides for MoS2 synthesis. Applied Surface Science, 2021, 535, 147684.	6.1	7
8	Deep learning STEM-EDX tomography of nanocrystals. Nature Machine Intelligence, 2021, 3, 267-274.	16.0	30
9	Atomic-scale chemical mapping of copper dopants in Bi2Te2.7Se0.3 thermoelectric alloy. Materials Today Physics, 2021, 17, 100347.	6.0	13
10	Evolution and expansion of Li concentration gradient during charge–discharge cycling. Nature Communications, 2021, 12, 3814.	12.8	40
11	Unveiling the Origin of Robust Ferroelectricity in Sub-2 nm Hafnium Zirconium Oxide Films. ACS Applied Materials & Interfaces, 2021, 13, 36499-36506.	8.0	24
12	3D-to-2D phase transformation through highly ordered 1D crystals from transition-metal oxides to dichalcogenides. Materials Today, 2021, 47, 38-44.	14.2	3
13	Ferroelectric switching in GeTe through rotation of lone-pair electrons by Electric field-driven phase transition. Applied Materials Today, 2021, 24, 101122.	4.3	7
14	Area‣elective Atomic Layer Deposition of MoS <sub>2</sub> using Simultaneous Deposition and Etching Characteristics of MoCl <sub>5</sub> . Physica Status Solidi - Rapid Research Letters, 2021, 15, 2000533.	2.4	7
15	Facile and versatile ligand analysis method of colloidal quantum dot. Scientific Reports, 2021, 11, 19889.	3.3	1
16	In-depth study of the chemical/electronic structures of two-dimensional molybdenum disulfide materials with sub-micrometer-resolution scanning photoelectron microscopy. 2D Materials, 2020, 7, 025002.	4.4	9
17	Intriguing morphological evolution during chemical vapor deposition of HfS2 using HfCl4 and S on sapphire substrate. Applied Surface Science, 2020, 509, 144701.	6.1	5
18	Introduction of an Al Seed Layer for Facile Adsorption of MoCl <sub>5</sub> during Atomic Layer Deposition of MoS <sub>2</sub> . Physica Status Solidi (A) Applications and Materials Science, 2020, 217, 1901042.	1.8	6

#	Article	IF	CITATIONS
19	Elucidating the influence of residual polymer and gas environment on the electronic structure of a graphene layer using in situ APXPS. Applied Surface Science, 2020, 528, 146764.	6.1	0
20	Reliability of Industrial grade Embedded-STT-MRAM. , 2020, , .		3
21	Revealing unique energy level alignment at graphene/MoS2 2-dimensional layered junction using in situ ambient pressure x-ray photoelectron spectroscopy. 2D Materials, 2020, 7, 045012.	4.4	0
22	Ultrathin monolithic HfO2 formed by Hf-seeded atomic layer deposition on MoS2: Film characteristics and its transistor application. Thin Solid Films, 2019, 673, 112-118.	1.8	12
23	Non-equilibrium fractal growth of MoS <sub>2</sub> for electrocatalytic hydrogen evolution. CrystEngComm, 2019, 21, 478-486.	2.6	10
24	Amorphous FeZr metal for multi-functional sensor in electronic skin. Npj Flexible Electronics, 2019, 3,	10.7	18
25	Inverse Stranski–Krastanov Growth in Single-Crystalline Sputtered Cu Thin Films for Wafer-Scale Device Applications. ACS Applied Nano Materials, 2019, 2, 3300-3306.	5.0	3
26	Lamellar-structured Ni-silicide film formed by eutectic solidification. Journal of Alloys and Compounds, 2019, 771, 124-130.	5.5	1
27	Microstructural visualization of compositional changes induced by transition metal dissolution in Ni-rich layered cathode materials by high-resolution particle analysis. Nano Energy, 2019, 56, 434-442.	16.0	132
28	Observation of heterostructure epitaxy of Pt-doped Ni-monosilicide on Si(001). Microelectronic Engineering, 2019, 205, 14-19.	2.4	0
29	Misorientationâ€Angleâ€Dependent Phase Transformation in van der Waals Multilayers via Electronâ€Beam Irradiation. Advanced Materials, 2018, 30, e1706864.	21.0	10
30	Direct Three-Dimensional Observation of Core/Shell-Structured Quantum Dots with a Composition-Competitive Gradient. ACS Nano, 2018, 12, 12109-12117.	14.6	15
31	Environment-dependent and anion-vacancy-controlled reversible phase transition of MoS <sub>2</sub> synthesized by chemical vapor deposition. 2D Materials, 2018, 5, 041002.	4.4	1
32	Chemical/morphological transition behavior of lithium phosphorus oxynitride solid-electrolyte in air: An analytical approach based on X-ray photoelectron spectroscopy and atomic force microscopy. Journal of Power Sources, 2018, 399, 231-237.	7.8	7
33	Highly Flexible and Transparent Ag Nanowire Electrode Encapsulated with Ultra-Thin Al2O3: Thermal, Ambient, and Mechanical Stabilities. Scientific Reports, 2017, 7, 41336.	3.3	85
34	Chemically Homogeneous and Thermally Robust Ni <sub>1–<i>x</i></sub> Pt <sub><i>x</i></sub> Si Film Formed Under a Non-Equilibrium Melting/Quenching Condition. ACS Applied Materials & Interfaces, 2017, 9, 566-572.	8.0	5
35	Synthesis of Vertical MoO <sub>2</sub> /MoS <sub>2</sub> Core–Shell Structures on an Amorphous Substrate via Chemical Vapor Deposition. Journal of Physical Chemistry C, 2017, 121, 27693-27699.	3.1	20
36	3D reconstruction modeling of bulk heterojunction organic photovoltaic cells: Effect of the complexity of the boundary on the morphology. Journal of the Korean Physical Society, 2016, 68, 474-481.	0.7	0

#	Article	IF	CITATIONS
37	High mobility and high stability glassy metal-oxynitride materials and devices. Scientific Reports, 2016, 6, 23940.	3.3	24
38	Ar plasma treated ZnON transistor for future thin film electronics. Applied Physics Letters, 2015, 107, .	3.3	52
39	45.3: <i>Invited Paper</i> : High Performance Nanocrystalline ZnO <sub>x</sub> N <sub>y</sub> for Imaging and Display Applications. Digest of Technical Papers SID International Symposium, 2015, 46, 681-684.	0.3	0
40	Wafer-scale synthesis of thickness-controllable MoS <sub>2</sub> films via solution-processing using a dimethylformamide/n-butylamine/2-aminoethanol solvent system. Nanoscale, 2015, 7, 9311-9319.	5.6	82
41	Auger electron nanoscale mapping and x-ray photoelectron spectroscopy combined with gas cluster ion beam sputtering to study an organic bulk heterojunction. Applied Physics Letters, 2014, 104, 243303.	3.3	6
42	Origin of High Photoconductive Gain in Fully Transparent Heterojunction Nanocrystalline Oxide Image Sensors and Interconnects. Advanced Materials, 2014, 26, 7102-7109.	21.0	65
43	Photocarrier dynamics near V-shaped pits in InxGa1â^'xN/GaN multiple quantum wells. Chemical Physics, 2014, 436-437, 51-54.	1.9	2
44	Nanocrystalline ZnON; High mobility and low band gap semiconductor material for high performance switch transistor and image sensor application. Scientific Reports, 2014, 4, 4948.	3.3	82
45	Ultrafast photocarrier dynamics in nanocrystalline ZnO_xN_y thin films. Optics Letters, 2014, 39, 5062.	3.3	4
46	Influence of V-pits on the efficiency droop in InGaN/GaN quantum wells. Optics Express, 2014, 22, A857.	3.4	64
47	A Flexible Bimodal Sensor Array for Simultaneous Sensing of Pressure and Temperature. Advanced Materials, 2014, 26, 796-804.	21.0	375
48	Anion control as a strategy to achieve high-mobility and high-stability oxide thin-film transistors. Scientific Reports, 2013, 3, 1459.	3.3	137
49	Epitaxial growth technology for optical interconnect based on bulk-Si platform. , 2013, , .		1
50	High mobility zinc oxynitride-TFT with operation stability under light-illuminated bias-stress conditions for large area and high resolution display applications. , 2012, , .		17
51	Gated three-terminal device architecture to eliminate persistent photoconductivity in oxide semiconductor photosensor arrays. Nature Materials, 2012, 11, 301-305.	27.5	434
52	Evaluation of Optical Waveguide by Solid Phase Epitaxial Growth of Amorphous Silicon. ECS Transactions, 2012, 41, 19-25.	0.5	0
53	Local structure and local conduction paths in amorphous (In,Ga,Hf)–ZnO semiconductor thin films. Solid State Communications, 2012, 152, 1867-1869.	1.9	5
54	Density of States-Based Design of Metal Oxide Thin-Film Transistors for High Mobility and Superior Photostability. ACS Applied Materials & Interfaces, 2012, 4, 5416-5421.	8.0	63

#	Article	IF	CITATIONS
55	Dual gate photo-thin film transistor with high photoconductive gain for high reliability, and low noise flat panel transparent imager. , 2011, , .		4
56	Nanometer-Scale Oxide Thin Film Transistor with Potential for High-Density Image Sensor Applications. ACS Applied Materials & Interfaces, 2011, 3, 1-6.	8.0	70
57	Ne[sup +] ion sputtering effect on amorphous Ga-In-Zn-O thin-film surface investigated by high-resolution XPS. AIP Conference Proceedings, 2011, , .	0.4	Ο
58	Sputtering Effect on Amorphous Ga–In–Zn–O Thin-Film Surface: Occurrence of Subgap and Metallic States. Electrochemical and Solid-State Letters, 2010, 13, H454.	2.2	8
59	Ti/Cu bilayer electrodes for SiNx-passivated Hf–In–Zn–O thin film transistors: Device performance and contact resistance. Applied Physics Letters, 2010, 97, 162105.	3.3	27
60	180nm gate length amorphous InGaZnO thin film transistor for high density image sensor applications. , 2010, , .		19
61	Effect of oxygen partial pressure on the Fermi level of ZnO1â^'x films fabricated by pulsed laser deposition. Applied Physics Letters, 2010, 96, 201907.	3.3	36
62	Novel stress-memorization-technology (SMT) for high electron mobility enhancement of gate last high-k/metal gate devices. , 2010, , .		11
63	Characteristics and Cleaning of Dry-Etching-Damaged Layer of Amorphous Oxide Thin-Film Transistor. Electrochemical and Solid-State Letters, 2009, 12, H95.	2.2	17
64	Source/Drain Formation of Self-Aligned Top-Gate Amorphous GaInZnO Thin-Film Transistors by \$hbox{NH}_{3}\$ Plasma Treatment. IEEE Electron Device Letters, 2009, 30, 374-376.	3.9	54
65	Amorphous hafnium-indium-zinc oxide semiconductor thin film transistors. Applied Physics Letters, 2009, 95, .	3.3	217
66	Investigations of semiconductor devices using SIMS; diffusion, contamination, process control. Applied Surface Science, 2008, 255, 1395-1399.	6.1	11
67	Short Channel Characteristics of Gallium–Indium–Zinc–Oxide Thin Film Transistors for Three-Dimensional Stacking Memory. IEEE Electron Device Letters, 2008, 29, 549-552.	3.9	80
68	High performance oxide thin film transistors with double active layers. , 2008, , .		27
69	Source/Drain Series-Resistance Effects in Amorphous Gallium–Indium Zinc-Oxide Thin Film Transistors. IEEE Electron Device Letters, 2008, 29, 879-881.	3.9	92
70	High-performance amorphous gallium indium zinc oxide thin-film transistors through N2O plasma passivation. Applied Physics Letters, 2008, 93, .	3.3	112
71	Self-aligned top-gate amorphous gallium indium zinc oxide thin film transistors. Applied Physics Letters, 2008, 93, .	3.3	89
72	Selection of α variants during microstructural evolution in <b><i>α/β</i></b> titanium alloys. Philosophical Magazine, 2007, 87, 3615-3627.	1.6	84

#	Article	IF	CITATIONS
73	New Approach for Passivation of Ga <inf>2</inf> O <inf>3</inf> -In <inf>2</inf> O <inf>3</inf> -ZnO Thin Film Transistors. , 2007, , .		1
74	Highly Manufacturable Single Metal Gate Process Using Ultra-Thin Metal Inserted Poly-Si Stack (UT-MIPS). , 2006, , .		4
75	Highly Stable Ga2O3-In2O3-ZnO TFT for Active-Matrix Organic Light-Emitting Diode Display Application. , 2006, , .		16
76	Modeling the tensile properties in β-processed α/β Ti alloys. Metallurgical and Materials Transactions A: Physical Metallurgy and Materials Science, 2006, 37, 559-566.	2.2	66
77	High trap density and long retention time from self-assembled amorphous Si nanocluster floating gate nonvolatile memory. Applied Physics Letters, 2006, 89, 243513.	3.3	6
78	Direct observations of dislocation substructures formed by nano-indentation of the α-phase in an α/β titanium alloy. Materials Science & Engineering A: Structural Materials: Properties, Microstructure and Processing, 2005, 400-401, 463-466.	5.6	8
79	Direct observations and analyses of dislocation substructures in the α phase of an α/β Ti-alloy formed by nanoindentation. Acta Materialia, 2005, 53, 5101-5115.	7.9	93
80	Rapid characterization of titanium microstructural features for specific modelling of mechanical properties. Measurement Science and Technology, 2005, 16, 60-69.	2.6	54
81	Quantification of microstructural features in α/β titanium alloys. Materials Science & Engineering A: Structural Materials: Properties, Microstructure and Processing, 2004, 372, 191-198.	5.6	175
82	3D Materials Characterization using Dual-Beam FIB/SEM Techniques. Microscopy and Microanalysis, 2004, 10, 1128-1129.	0.4	5
83	Fabrication and phase-transformation issues in CTFF-MA processed A15 superconductors. AIP Conference Proceedings, 2002, , .	0.4	4
84	Analysis of eddy current AC loss for untwisted, multifilamentary superconducting composites with various aspect ratios. IEEE Transactions on Applied Superconductivity, 2001, 11, 2963-2966.	1.7	2
85	Magnetization as a critical defining parameter for strand in precision dipole applications implications for field error and F-J stability. IEEE Transactions on Applied Superconductivity, 2001, 11, 2567-2570.	1.7	13